

Membership Inference Attacks against Generative Models with Probabilistic Fluctuation

Wenjie Fu¹, Huandong Wang², Chen Gao², Guanghua Liu¹, Yong Li² and Tao Jiang¹

¹Huazhong University of Science and Technology

²Tsinghua University

wjfu99@outlook.com, {wanghuandong, chgao96, liyong07}@tsinghua.edu.cn,
{guanghualiu, taojiang}@hust.edu.cn

Abstract

Membership Inference Attack (MIA) identifies whether a record exists in a machine learning model’s training set by querying the model. MIAs on the classic classification models have been well-studied, and recent works have started to explore how to transplant MIA onto generative models. Our investigation indicates that existing MIAs designed for generative models mainly depend on the overfitting in target models. However, overfitting can be avoided by employing various regularization techniques, whereas existing MIAs demonstrate poor performance in practice. Unlike overfitting, memorization is essential for deep learning models to attain optimal performance, making it a more prevalent phenomenon. Memorization in generative models leads to an increasing trend in the probability distribution of generating records around the member record. Therefore, we propose a **Probabilistic Fluctuation Assessing Membership Inference Attack (PFAMI)**, a novel MIA that infers memberships by detecting these trends via analyzing the overall probabilistic fluctuations around given records. We conduct extensive experiments across multiple generative models and datasets, which demonstrate PFAMI can improve the attack success rate (ASR) by about 27.9% when compared with the best baseline. Besides, our code and datasets are available at the following link¹.

1 Introduction

In recent years, fueled by abundant data resources and empowered by deep neural networks, generative models have achieved remarkable success in various domains such as computer vision [Rombach *et al.*, 2022], natural language processing [Li *et al.*, 2021], and spatial-temporal data modeling [Tashiro *et al.*, 2021]. These generative models have the capability to generate authentic and creative content, which has prompted the deployment of various generative services [Stokel-Walker and Van Noorden, 2023].

¹<https://github.com/wjfu99/MIA-Gen>

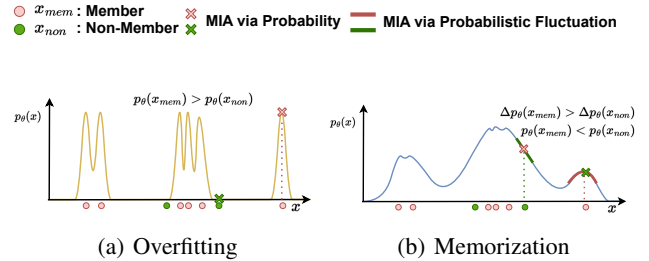


Figure 1: MIAs against generative models with overfitting and memorization. Identifying member records based on probability is feasible on overfitting models but fails on models only with memorization. Memorization arises as an increased tendency in probability density around member records, which can be captured by estimating the fluctuation of probability.

However, while we enjoy the revolutionary benefits that these services bring, we also face various increasing privacy risks [Bommasani *et al.*, 2021] and copyright disputes [Epstein *et al.*, 2023]. For example, the model privacy can be exposed to malicious users through the generative services [Hayes *et al.*, 2019; Zhang *et al.*, 2020]. On the other side, unauthorized content may be secretly utilized to construct generative services [Dwivedi *et al.*, 2023].

Existing works have revealed privacy leakage in generative models from multiple perspectives. Membership inference attacks (MIAs) aim to identify the membership of a given record as the member record that comes from the training set, or as the non-member record that comes from a disjoint set [Shokri *et al.*, 2017]. MIAs have been widely explored in the classic classification tasks and represent tremendous privacy leakage [Hu *et al.*, 2022]. Recently, some preliminary researches have conducted MIAs on generative models. They essentially use different metrics as the proxy to approximate the probability of a specific record being generated by the target model, then infer memberships based on the magnitude of aforementioned probability [Hu *et al.*, 2022]. For example, some works [Hilprecht *et al.*, 2019; Chen *et al.*, 2020; Liu *et al.*, 2019] employ the minimum distance between generated records and the target record as a metric for approximating the aforementioned probability. Other works [Hayes *et al.*, 2019; Hu and Pang, 2021] utilize the confidence values outputted by the discriminator to serve as a proxy for this probability.

However, the current attack paradigm has a notable flaw.

Specifically, these methods heavily depend on overfitting in target generation models. As demonstrated in Figure 1(a), overfitting prompts member records to strike overall higher probabilities of being generated than non-member ones. Thus, probability can be utilized as an indicator for membership inference. However, training techniques such as regularization and early-stopping are widely adopted for eliminating overfitting [Ying, 2019]. Consequently, deep learning models are usually overfitting-free, and the performance of existing attack algorithms in practical scenarios cannot be guaranteed. In contrast, deep learning models inevitably exhibit phenomena of memorization [Feldman and Zhang, 2020]. As shown in Figure 1(b), memorization in generative models causes an increased tendency of probability density when the record closely resembles a member record [van den Burg and Williams, 2021]. Therefore, we consider a more practical and promising attack framework that captures the feature of memorization by estimating the fluctuation of probability within the local scopes of data records.

Nevertheless, three challenges need to be addressed before bringing this framework to a practical MIA. Firstly, both conventional probability-based and our proposed probabilistic fluctuation-based attack framework rely on the proxy for approximating probabilities. However, existing proxies either rely on massive synthetic records [van Breugel *et al.*, 2023] or are only applicable in white-box settings [Chen *et al.*, 2020]. Therefore, the first challenge is estimating the probability in an efficient manner without requiring massive synthetic records. Furthermore, the probabilistic fluctuations around the target sample are highly complex within the high-dimensional data space. Specifically, the fluctuations exhibit significant variations in different directions, and the fluctuations also differ at varying distances in the same direction. Therefore, the second challenge is how to generate representative neighbor records from an appropriate direction and various distances to depict the adjacent probabilistic fluctuations. The final challenge lies in how to design the inference function that quantifies and aggregates the probabilistic fluctuations from multiple neighbors, in order to obtain an indicator that can effectively distinguish between members and non-members.

In this paper, we propose the **Probabilistic Fluctuation Assessing Membership Inference (PFAMI)** composed with three elaborately designed modules to address these challenges. First, we design an effective probability estimation method based on variational inference, which is feasible on probabilistic generative models, such as variational autoencoders (VAEs) and diffusion models (DMs), with several synthetic records. Furthermore, we propose a dynamic perturbation mechanism that can obtain an ensemble of representative neighbor records in the local scope by adjusting the strength of the perturbation. This ensemble paves the way for comprehensively characterizing the distribution of probabilistic fluctuations around the target record. Finally, based on the distribution of probabilistic fluctuations, we design a statistical metric-based as well as a neural networks (NNs)-based inference function to extract the distinctive memorization features for distinguishing between members and non-members.

Overall, our contributions are summarized as follows:

Table 1: Taxonomy of MIAs against generative models. \otimes and \odot denote the w/ or w/o access requirements of specific parts. \square and \blacksquare indicate white-box and black-box accesses of specific parts. \checkmark and \times represent whether an attacking algorithm is feasible for the corresponding generative model. Synthetic denotes a large-scale generated dataset prepared for MIAs in advance.

Method	Access			Applicable			
	Generator	Discriminator	Synthetic	Overfitting	Memorization	DMs	VAEs
Co-Membership Attack	\square	\otimes	\otimes	\checkmark	\times	\checkmark	\checkmark
GAN-Leaks (White-Box)	\square	\otimes	\otimes	\checkmark	\times	\checkmark	\checkmark
Over-Representation (O-R)	\blacksquare	\odot	\otimes	\checkmark	\times	\times	\times
LOGAN	\blacksquare	\odot	\otimes	\checkmark	\times	\times	\times
(O-R) + Surrogate Model	\blacksquare	\otimes	\odot	\checkmark	\times	\checkmark	\checkmark
LOGAN + Surrogate Model	\blacksquare	\otimes	\odot	\checkmark	\times	\checkmark	\checkmark
Monte-Carlo Set	\blacksquare	\otimes	\odot	\checkmark	\times	\checkmark	\checkmark
GAN-Leaks (Black-Box)	\blacksquare	\otimes	\otimes	\checkmark	\times	\checkmark	\checkmark
SecMI _{DM}	\blacksquare	\otimes	\otimes	\checkmark	\times	\checkmark	\times
SecMI _{VAE}	\blacksquare	\otimes	\otimes	\checkmark	\times	\checkmark	\times
PFAMI _{DM}	\blacksquare	\otimes	\otimes	\checkmark	\checkmark	\checkmark	\checkmark
PFAMI _{VAE}	\blacksquare	\otimes	\otimes	\checkmark	\checkmark	\checkmark	\checkmark

- We demonstrate that detecting memorization sheds light on MIAs against overfitting-free generative models and propose a framework that detects the distinctive characteristics of member records memorized by the target model from the perspective of probabilistic fluctuations.
- We propose PFAMI, a novel MIA method that incorporates a probability estimation approach via variational inference and a dynamic perturbation mechanism to characterize the distribution of probabilistic fluctuations, and two elaborately designed inference functions, including a metric-based approach and an NNs-based approach, to extract essential features for membership inference attack.
- We conducted extensive experiments to validate the effectiveness of PFAMI. The results suggest that PFAMI shows significantly higher ASR and stability across multiple generation models and datasets compared with existing MIAs (about 19.8% and 35.9% improvement in ASR on diffusion models and VAEs, respectively).

2 Related Works

Generative Models With the development of deep learning, massive deep generative models are proposed for generating authentic data samples [Oussidi and Elhassouny, 2018]. VAEs [Kingma and Welling, 2014; Higgins *et al.*, 2017], a family of preliminary generative models, incorporate an encoder network to map the original data distribution into a Gaussian distribution and a decoder to generate reconstructed data from the latent distribution. Recently, diffusion models [Ho *et al.*, 2020; Song *et al.*, 2021] explore to construct desired data samples from the noise by learning a parameterized denoising process in a Markov chain. They become a new family of state-of-the-art generative models and achieve a dominant position in generative tasks such as image generation [Rombach *et al.*, 2022], text generation [Li *et al.*, 2021], and spatial-temporal data imputation [Tashiro *et al.*, 2021]. In this work, we elaborately evaluate the vulnerabilities of both VAEs and diffusion models to existing MIAs and PFAMI.

Membership Inference Attack Shokri *et al.* formally proposed the MIAs, which aim to determine if a specific data record was included in the training set of a target model. Previous studies on Membership Inference Attacks have primarily concentrated on classification tasks [Choquette-Choo *et al.*, 2021]. Recently, with the emergence of generative mod-

els, researchers have focused on exploring their vulnerabilities regarding MIA. As the taxonomy summarized in Table 1, several studies [Chen *et al.*, 2020; Liu *et al.*, 2019] assume a white-box access of generators and search the smallest distance between the target record and generated records via the first-order optimization. Other works with black-box access measure this distance through a massive synthetic dataset generated by the target model [Hilprecht *et al.*, 2019]. Additionally, there are specific studies that employ the discriminator’s confidence value as a metric to differentiate member and non-member records [Hayes *et al.*, 2019; Hu and Pang, 2021], while others adopt the estimation error [Duan *et al.*, 2023]. However, existing methods are only feasible on models with overfitting, and fail on models only with memorization. On the contrary, our approach infers the memberships by detecting distinctive characteristics of the training records memorized by the target model, leading to outstanding attack performance and reduced access requirements. Notably, a contemporary study proposes an MIA, neighbor attack [Mattern *et al.*, 2023], for language models. While neighbor attack and PFAMI exhibit some similarities in implementations, they are fundamentally based on distinct intuitions. The PFAMI methodology is driven by the inherent phenomena in generative models, which offer profound theoretical underpinnings. Conversely, the neighbor attack suggests counteracting the bias caused by the inherent complexity of the target text by comparing it with neighboring samples.

3 Preliminary

In this section, we introduce representative generative models and present a formal definition of a gray-box threat model. The key notations utilized in this paper will be described in Appendix A.1.

3.1 Generative Models

In this work, we focus on the probabilistic deep generative models, which include diffusion models [Ho *et al.*, 2020] and VAEs [Kingma and Welling, 2014], as these are more amenable to direct analysis of the learned probability.

VAEs has the similar structure as an autoencoder [Zhai *et al.*, 2018], which is composed of two modules: probabilistic encoder $q_\phi(\mathbf{z}|\mathbf{x})$ and decoder $p_\theta(\mathbf{x}|\mathbf{z})$. The approximate posterior is a multivariate Gaussian distribution parameterized by encoder ϕ :

$$q_\phi(\mathbf{z}|\mathbf{x}) = \mathcal{N}(\mathbf{z}; \boldsymbol{\mu}_\phi(\mathbf{x}), \boldsymbol{\sigma}_\phi^2(\mathbf{x}) \mathbf{I}), \quad (1)$$

where $\boldsymbol{\mu}_\phi$ and $\boldsymbol{\sigma}_\phi$ are calculated by the encoding neural networks with the input of \mathbf{x} .

$p_\theta(\mathbf{x}|\mathbf{z})$ is a multivariate Gaussian or Bernoulli distribution depending on the type of data. In the image generation task, it is set to be a Gaussian distribution:

$$p_\theta(\mathbf{x}|\mathbf{z}) = \mathcal{N}(\mathbf{x}; \boldsymbol{\mu}_\theta(\mathbf{z}), \boldsymbol{\sigma}_\theta^2(\mathbf{z}) \mathbf{I}), \quad (2)$$

where $\boldsymbol{\mu}_\theta$ and $\boldsymbol{\sigma}_\theta$ are calculated by the decoding neural networks with the input of the latent code \mathbf{z} .

Unlike VAEs, diffusion models are learned with a fixed encoding procedure. Diffusion models includes T steps forward

diffusion process $q(\mathbf{x}_t | \mathbf{x}_{t-1})$ and reverse denoising process $p_\theta(\mathbf{x}_{t-1} | \mathbf{x}_t)$, which can be respectively formulated as:

$$\begin{aligned} q(\mathbf{x}_t | \mathbf{x}_{t-1}) &= \mathcal{N}(\mathbf{x}_t; \sqrt{1 - \beta_t} \mathbf{x}_{t-1}, \beta_t \mathbf{I}) \\ p_\theta(\mathbf{x}_{t-1} | \mathbf{x}_t) &= \mathcal{N}(\mathbf{x}_{t-1}; \boldsymbol{\mu}_\theta(\mathbf{x}_t, t), \boldsymbol{\sigma}_\theta(\mathbf{x}_t, t)), \end{aligned} \quad (3)$$

where $\{\beta_t \in (0, 1)\}_{t=1}^T$ is the variance schedule. Besides, in the forward process, there is a nice property that allows sampling \mathbf{x}_t at any arbitrary time step t :

$$\mathbf{x}_t(\mathbf{x}_0, \boldsymbol{\epsilon}) = \sqrt{\bar{\alpha}_t} \mathbf{x}_0 + \sqrt{1 - \bar{\alpha}_t} \boldsymbol{\epsilon}, \quad (4)$$

where $\alpha_t = 1 - \beta_t$, $\bar{\alpha}_t = \prod_{i=1}^t \alpha_i$ and $\boldsymbol{\epsilon} \sim \mathcal{N}(\mathbf{0}, \mathbf{I})$. It is also noteworthy that the reverse probability is tractable when conditioned on \mathbf{x}_0 :

$$q(\mathbf{x}_{t-1} | \mathbf{x}_t, \mathbf{x}_0) = \mathcal{N}(\mathbf{x}_{t-1}; \tilde{\boldsymbol{\mu}}_t(\mathbf{x}_t, \mathbf{x}_0), \tilde{\boldsymbol{\beta}}_t \mathbf{I}), \quad (5)$$

where $\tilde{\boldsymbol{\mu}}_t(\mathbf{x}_t, \mathbf{x}_0) := \frac{\sqrt{\bar{\alpha}_{t-1}} \beta_t}{1 - \bar{\alpha}_t} \mathbf{x}_0 + \frac{\sqrt{\alpha_t} (1 - \bar{\alpha}_{t-1})}{1 - \bar{\alpha}_t} \mathbf{x}_t$ and $\tilde{\beta}_t := \frac{1 - \bar{\alpha}_{t-1}}{1 - \bar{\alpha}_t} \beta_t$.

3.2 Threat Model

In this work, we consider an adversary that attempts to infer whether a specific data record was used in the training phase of the target generative model. Three mainstream attack scenarios considered in existing works are white-box [Carlini *et al.*, 2023], black-box [Hilprecht *et al.*, 2019], and gray-box [Duan *et al.*, 2023]. In the white-box scenario, the adversary has full access to the target model, including the internal parameters of target models. However, in the black-box scenario, the attacker can only receive ultimate synthetic results and lacks knowledge of the internal workings mechanism. The gray-box scenario typically necessitates access to intermediate results of target models compared to black-box attacks, which is a practical scenario where some service providers retain ownership of models’ parameters while allowing users to manipulate the intermediate synthetic results [Chen *et al.*, 2020; Pang and Wang, 2023], such as the latent codes in VAEs and the unfinished denoised images in diffusion models. Therefore, we adopt the gray-box scenario in this research to evaluate our proposed method in a realistic manner. D is a dataset drawn from the real data distribution, which can be partitioned into two separate subsets: D_{mem} and D_{non} . The target model θ is trained on D_{mem} , and the adversary is unaware of which data records are included in the training set D_{mem} . Formally, the adversary algorithm \mathcal{A} is designed to predicted whether a data record $\mathbf{x}^{(i)} \in D$ is in the training dataset D_{mem} :

$$\mathcal{A}(\mathbf{x}^{(i)}, \theta) = \mathbb{1} \left[P(m^{(i)} = 1 | \mathbf{x}^{(i)}, \theta) \geq \tau \right], \quad (6)$$

where $m^{(i)} = 1$ indicates that the record $\mathbf{x}^{(i)} \in D_{mem}$, τ denotes the threshold, $\mathbb{1}$ is the indicator function.

4 Methodology

As shown in Figure 2, we introduce a novel MIA framework, which infers memberships by employing probabilistic fluctuation assessment. Subsequently, we design three modules to address three challenges posed by this framework.

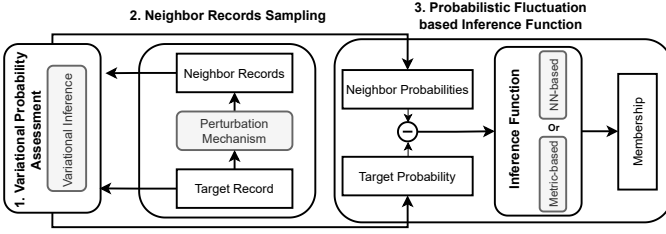


Figure 2: The overall framework of PFAMI and the three modules introduced to deploy it in practice.

4.1 Framework

The objective of a generative model is to learn a latent variable model $p_\theta(\mathbf{x})$ to approximate the genuine data distribution $q(\mathbf{x})$. Thus, as we discuss in Sec. 1, there is an attack framework widely adopted by existing MIAs against generative models that approximates the probabilities of target records being generated and then sets a threshold to discriminate between member and non-member records. This framework highly relies on the overfitting phenomenon in target models that drives member records more likely to be generated than non-member records. Besides, in the training pipeline of generative models, techniques like early stopping and regularization are widely used to prevent overfitting and improve generalization [Ying, 2019], which exacerbates the impracticality of this framework. Formally, the **existing attack framework** can be formulated as:

$$\mathcal{A}_{exist}(\mathbf{x}^{(i)}, \theta) = \mathbb{1} \left[\hat{p}_\theta(\mathbf{x}^{(i)}) \geq \tau \right], \quad (7)$$

where $\hat{p}_\theta(\mathbf{x}^{(i)})$ is the approximate probability of $\mathbf{x}^{(i)}$ being generated.

Compared to overfitting, memorization is inevitable for achieving nearly optimal generalization on deep learning models [Feldman, 2020]. In generative models with memorization, member records tend to strike higher generative probabilities than neighbor records [van den Burg and Williams, 2021], i.e., it usually corresponds to a local maximum. Intuitively, we consider a more general attack framework that detects these local maximum points by leveraging the probabilistic fluctuations around target records. Thus, **our proposed framework** can be formally represented as:

$$\mathcal{A}_{our}(\mathbf{x}^{(i)}, \theta) = \mathbb{1} \left[\mathcal{F} \left(\left\{ \Delta \hat{p}_\theta(\mathbf{x}^{(i)}, \tilde{\mathbf{x}}_j^{(i)}) \right\}_{j=1}^M \right) \geq \tau \right], \quad (8)$$

where $\Delta \hat{p}_\theta(\mathbf{x}^{(i)}, \tilde{\mathbf{x}}_j^{(i)})$ represents the probabilistic fluctuation between the target record $\mathbf{x}^{(i)}$ and its neighbor record $\tilde{\mathbf{x}}_j^{(i)}$. M indicates the number of neighbor records, $\mathcal{F}(\cdot)$ is an inference function that can qualify the overall probabilistic fluctuation around the target record $\mathbf{x}^{(i)}$.

To implement our proposed framework in practical applications, we introduce three new modules sequentially. As depicted in Figure 2, we first propose a variational probability assessment approach to efficiently approximate the probability $\hat{p}_\theta(\mathbf{x}^{(i)})$ of the record $\mathbf{x}^{(i)}$ being generated. Then we design a dynamic perturbation mechanism to sample representative neighbors within the local scope for estimating

$\Delta \hat{p}_\theta(\mathbf{x}^{(i)}, \tilde{\mathbf{x}}_j^{(i)})$. Finally, we introduce two strategies with two inference functions to identify member records.

4.2 Variational Probability Assessment

Existing works estimate the probability $p_\theta(\mathbf{x})$ by calculating the smallest distance between the target record and the synthetic record set [Hu *et al.*, 2022]. Nevertheless, these approaches [Hayes *et al.*, 2019; Hilprecht *et al.*, 2019; van Breugel *et al.*, 2023] rely on tens of thousands of generated records, which leads to low efficiency.

We notice that probabilistic generative models, like diffusion models and VAEs, perform training by optimizing the evidence lower bound (ELBO) of $p_\theta(\mathbf{x})$. Therefore, we attempt to derive an approximate probability $\hat{p}_\theta(\mathbf{x}^{(i)})$ to estimate the relative value of $p_\theta(\mathbf{x})$ via variational inference.

Diffusion models: The ELBO can be written as:

$$\mathbb{E}_q \left[\log \frac{q(\mathbf{x}_{1:T} | \mathbf{x}_0)}{p_\theta(\mathbf{x}_{0:T})} \right] =: L_{ELBO} \geq -\log p_\theta(\mathbf{x}_0). \quad (9)$$

Ho *et al.* further rewrite L_{ELBO} to $\sum_{t=0}^T L_t$, where L_T is a constant can be ignored during optimization [Ho *et al.*, 2020]. $L_{1:T-1}$ represents the estimation error of \mathbf{x}_{t-1} , which can be expanded by applying Eq. (3) and Eq. (5):

$$\begin{aligned} L_{t-1}(\mathbf{x}_0) &= D_{KL}(q(\mathbf{x}_{t-1} | \mathbf{x}_t, \mathbf{x}_0) \| p_\theta(\mathbf{x}_{t-1} | \mathbf{x}_t)) \\ &= \mathbb{E}_q \left[\frac{1}{2\sigma_t^2} \|\tilde{\boldsymbol{\mu}}_t(\mathbf{x}_t, \mathbf{x}_0) - \boldsymbol{\mu}_\theta(\mathbf{x}_t, t)\|^2 \right], \end{aligned} \quad (10)$$

where the $\boldsymbol{\mu}_\theta$ is trained to predict $\tilde{\boldsymbol{\mu}}_t$ based on \mathbf{x}_t and t . For an attack model with the gray-box setting, it can calculate $\tilde{\boldsymbol{\mu}}_t(\mathbf{x}_t, \mathbf{x}_0)$ through the fixed forward diffusion process:

$$\tilde{\boldsymbol{\mu}}_t(\mathbf{x}_t, \mathbf{x}_0) = \frac{1}{\sqrt{\alpha_t}} \left(\mathbf{x}_t(\mathbf{x}_0, \epsilon) - \frac{\beta_t}{\sqrt{1 - \bar{\alpha}_t}} \epsilon \right), \quad (11)$$

where ϵ is sampled from $\mathcal{N}(\mathbf{0}, \mathbf{I})$, and $\mathbf{x}_t(\mathbf{x}_0, \epsilon)$ can be calculated by following Eq. (4). Then the attacker can acquire the expectation of predicted sample $\boldsymbol{\mu}_\theta(\mathbf{x}_t, t)$ based on Eq. (3) and Monte Carlo sampling:

$$\boldsymbol{\mu}_\theta(\mathbf{x}_t, t) \approx \sum_i \mathbf{x}_{t-1}^{(i)}, \quad (12)$$

where $\mathbf{x}_{t-1}^{(i)} \sim p_\theta(\mathbf{x}_{t-1} | \mathbf{x}_t)$. Thus, attacker can estimate the relative value of $p_\theta(\mathbf{x}_0)$ by fusing the estimation error across N sampled time steps:

$$\hat{p}_\theta(\mathbf{x}_0) := -\frac{1}{N} \sum_t^N L_t(\mathbf{x}_0), \quad (13)$$

where \log is ignored for simplification, and same operation is also performed for VAEs.

VAEs: The ELBO can be derived as the following two tractable items:

$$\begin{aligned} -\mathbb{E}_{\mathbf{z} \sim q_\phi(\mathbf{z} | \mathbf{x})} \log p_\theta(\mathbf{x} | \mathbf{z}) + D_{KL}(q_\phi(\mathbf{z} | \mathbf{x}) \| p_\theta(\mathbf{z})) \\ =: L_{ELBO} \geq -\log p_\theta(\mathbf{x}), \end{aligned} \quad (14)$$

where $\mathbb{E}_{\mathbf{z} \sim q_\phi(\mathbf{z} | \mathbf{x})} \log p_\theta(\mathbf{x} | \mathbf{z})$ maximizes the likelihood of generating real data record \mathbf{x} , $D_{KL}(q_\phi(\mathbf{z} | \mathbf{x}) \| p_\theta(\mathbf{z}))$ restricts

the estimated posterior $q_\phi(\mathbf{z}|\mathbf{x})$ mapped from the real data record close to the prior $p_\theta(\mathbf{z})$. Our adversary model is feasible to estimate both of them by only querying the target model without any knowledge of inherent parameters. The $\mathbb{E}_{\mathbf{z}\sim q_\phi} \log p_\theta$ can be represented as follows by applying the Monte Carlo sampling method and Eq. (2):

$$\begin{aligned} \mathbb{E}_{\mathbf{z}\sim q_\phi} \log p_\theta &= \frac{1}{N} \sum_{n=1}^N \log p_\theta(\mathbf{x} | \mathbf{z}^{(n)}) \\ &= \frac{1}{N} \sum_{n=1}^N \log \frac{1}{\sigma_\theta \sqrt{2\pi}} e^{-\frac{1}{2} \left(\frac{\mathbf{x} - \mathbf{x}^{(n)}}{\sigma_\theta} \right)^2} \\ &\propto - \sum_{n=1}^N \left\| \mathbf{x} - \mathbf{x}^{(n)} \right\|^2, \end{aligned} \quad (15)$$

where N represents the number of Monte Carlo sampling, $\mathbf{x}^{(n)}$ is the mean of the $p_\theta(\mathbf{x} | \mathbf{z}^{(n)})$, i.e., $\mathbf{x}^{(n)} = \boldsymbol{\mu}_\theta^{(n)}$, and it can be directly obtained by querying the target model. Since the decoder of the VAE calculates $\boldsymbol{\mu}_\theta(\mathbf{z}^{(n)})$ with neural networks, and outputs it as the reconstructed sample $\mathbf{x}^{(n)}$. $\|\mathbf{x} - \mathbf{x}^{(n)}\|^2$ is proportional to the mean squared error (MSE) between the original and reconstructed data records. $D_{\text{KL}}(q_\phi(\mathbf{z}|\mathbf{x})\|p_\theta(\mathbf{z}))$ can be calculated with a closed-form solution as it is the KL divergence between two Gaussian distribution:

$$D_{\text{KL}}(q_\phi\|p_\theta) = \frac{1}{2} (1 + \log \sigma_\phi^2(\mathbf{x}) - \sigma_\phi^2(\mathbf{x}) - \boldsymbol{\mu}_\phi^2(\mathbf{x})). \quad (16)$$

Thus, attacker can approximate $p_\theta(\mathbf{x})$ by applying Eq. (16) and Eq. (15) to Eq. (14):

$$\hat{p}_\theta(\mathbf{x}) := - \sum_{n=1}^N \|\mathbf{x} - \mathbf{x}^{(n)}\|^2 - D_{\text{KL}}(\mathcal{N}(\boldsymbol{\mu}_\phi, \sigma_\phi^2 \mathbf{I})\|\mathcal{N}(0, 1)). \quad (17)$$

Based on Eq. (13) and Eq. (17), the adversary can approximate the relative value of $p_\theta(\mathbf{x})$ by sending a few query requests to the target model.

4.3 Neighbor Records Sampling

As formulated in Eq. (8), for a given data record $\mathbf{x}^{(i)}$, we have to sample an ensemble of representative neighbor records $\{\tilde{\mathbf{x}}_j^{(i)}\}_{j=1}^M$. Thus, how to sample representative neighbor records for exploring the local scope of a given data record is critical for instantiating our approach. Considering neighbors approximately appressed with the target record is imperative, but the data distributions are often high-dimensional and wide. We should avoid sampling neighbors out-of-range and can therefore refrain from exploring meaningless domains. Therefore, we opt for a data perturbation method that is as simple as possible, resulting in a minor but observable shift in the data distribution. Inspired by the data augmentation techniques widely used in machine learning for improving the model performance and generalization through increasing the diversity of the dataset, we design various perturbation methods to sample neighbor records, including crop, rotation, downsampling, brightening, etc. Furthermore, we conducted

extensive experiments to investigate the attack performance over various perturbation methods to find the most effective perturbation direction. The related information can be found in Appendix A.5, and the results suggest utilizing crop as the default direction as it combines excellent performance and stability. Furthermore, we consider sampling neighbor records at different distances by adjusting the strength of perturbation to comprehensively characterize the probabilistic fluctuations around the target record. Formally, we propose a general dynamic perturbation mechanism \mathcal{M} with increasing perturbation strengths $\{\lambda_j\}_{j=1}^M$ on arbitrary perturbation method:

$$\{\tilde{\mathbf{x}}_j^{(i)}\}_{j=1}^M = \left\{ \mathcal{M}(\mathbf{x}^{(i)}, \lambda_j) \right\}_{j=1}^M. \quad (18)$$

4.4 Probabilistic Fluctuation based Inference Function

Based on the variational approximate probability introduced in Sec. 4.2, and the perturbation mechanism proposed in Sec. 4.3. In this section, we elaborately design two strategies with different inference functions to qualify the overall probabilistic fluctuation by analyzing the characteristics of probability changes among the neighbor records of the target record: the metric-based inference, $\text{PFAMI}_{\text{Met}}$, and the neural networks (NNs)-based inference, $\text{PFAMI}_{\text{NNs}}$.

Metric-based Inference Function

For each data record $\mathbf{x}^{(i)} \in D$, we sample M neighbor records with increasing perturbation strengths and then set the inference function \mathcal{F} to be statistical averaging to estimate the overall probabilistic fluctuation. Formally, $\text{PFAMI}_{\text{Met}}$ can be formulated as:

$$\mathcal{A}(\mathbf{x}^{(i)}, \theta) = \mathbb{1} \left[\left(\frac{1}{M} \sum_{j=1}^M \Delta \hat{p}_\theta(\mathbf{x}^{(i)}, \tilde{\mathbf{x}}_j^{(i)}) \right) \geq \tau \right], \quad (19)$$

where $\Delta \hat{p}_\theta(\mathbf{x}^{(i)}, \tilde{\mathbf{x}}_j^{(i)}) = \left(\hat{p}(\mathbf{x}^{(i)}) - \hat{p}(\tilde{\mathbf{x}}_j^{(i)}) \right) / \hat{p}(\mathbf{x}^{(i)})$. Besides, to provide an intuitive understanding, we demonstrate that the overall probabilistic fluctuation can be approximately interpreted as the second derivative, which is typically employed to locate critical points. Please refer to Appendix A.6 for a detailed demonstration. Note that each approximate probability $\hat{p}_\theta(\cdot)$ is measured by repeatedly querying the target model N times in VAE based on Eq. (17). In diffusion models, $\hat{p}_\theta(\cdot)$ is calculated by taking the average of estimation errors over N sampled time steps based on Eq. (13).

NNs-based Inference Function

Instead of qualifying the overall probabilistic fluctuation by directly taking an average across M neighbors and N sampled points, we calculate each $\Delta \hat{p}_\theta$ over them. Therefore, we can obtain a $M \times N$ matrix $\Delta \hat{p}_\theta(\mathbf{x}^{(i)})$ for each target record, which can be represented as an ‘‘image’’ that contains probabilistic fluctuation information around the target record. Then we adopted an NNs-based model $f_{\mathcal{A}}$ as the inference function \mathcal{F} to capture the information of probabilistic fluctuation variation on this image. Specifically, convolutional

neural networks (CNNs)-based binary classification models are feasible to handle this task. In this manner, our proposed PFAMI_{NNs} can be formally represented as:

$$\mathcal{A}(\mathbf{x}^{(i)}, \theta) = \mathbb{1} \left[f_{\mathcal{A}} \left(\Delta \hat{p}_{\theta}(\mathbf{x}^{(i)}) \right) \geq \tau \right], \quad (20)$$

where $f_{\mathcal{A}}(\cdot)$ indicates the probability that PFAMI_{NNs} identify target record $\mathbf{x}^{(i)}$ as a member. Notably, our method does not follow existing studies [Duan *et al.*, 2023] that assume having access to an extensive number of ground truth labels for member and non-member records from the target model. Instead, we use an auxiliary dataset to train a shadow model to provide training samples for training our attack model. Then we deploy the trained attack model to infer memberships on the target model. Our method, in this manner, alleviates rigid assumptions, providing increased adaptability and practical applicability.

Clearly, the number of sampling records, N , and the number of neighbor records, M , jointly affect the total required query number $(M + 1) \times N$ for the inference attack. Therefore, choosing appropriate parameters for M and N helps strike a balance between improving attack performance and mitigating risks that may trigger the service provider’s risk management procedure. Thus, we perform experimental evaluations of the performance of PFAMI under different query numbers. For detailed information, please refer to the Appendix A.5.

To strike a more accurate probabilistic fluctuation estimation, we train a reference generative model with another relevant but disjoint dataset to calibrate the approximate probability $\hat{p}_{\theta}(\mathbf{x}_0)$ in both two strategies.

5 Experiments

5.1 Settings and Implementation Details

Datasets and Target models

We conduct experiments on two widely-used image datasets, Celeba-64 [Liu *et al.*, 2015] and Tiny-ImageNet (Tiny-IN) [Le and Yang, 2015]. For both datasets, we randomly select about 30% of all data samples for training and evaluating the target generative models, then utilize the rest for training the shadow and reference models. For example, Celeba-64 contains 202,599 images, whereas we respectively take 50,000 and 10,000 images as training and evaluation sets for target models. Notably, we make every effort to use all the data samples in each dataset to ensure that the target model has sufficiently large training samples since the limited member size will exacerbate the overfitting effect. For the target models, we adopted the two most representative generative models, DDPM [Ho *et al.*, 2020] and vanilla VAE [Kingma and Welling, 2014], to represent diffusion models and VAEs as well. Additionally, we also evaluated our proposed MIA against six state-of-the-art variant diffusion models and VAEs. It is worth noting that all models employ various regularization mechanisms to avoid overfitting. The detailed implementation information is summarized in Appendix A.2.

Baselines

We choose six state-of-the-art MIAs designed for generative models across all adversary scenarios to evaluate our proposed method comprehensively. There are two baselines set up in the white-box setting: Co-Membership [Liu *et al.*, 2019] and GAN-Leaks (White-Box) [Chen *et al.*, 2020]. Additionally, four baseline methods are employed for the black-box access scenario: LOGAN [Hayes *et al.*, 2019], Monte-Carlo Set [Hilprecht *et al.*, 2019], Over-Representation [Hu and Pang, 2021], and GAN-Leaks (Black-box) [Chen *et al.*, 2020]. Besides, SecMI [Duan *et al.*, 2023] represents the attack under gray-box access, which shares exactly the same setting as our proposed method. These baselines have been comprehensively verified to have appreciable attack performances over multifarious generative models and across myriad datasets.

5.2 Attack Performance

As shown in Table 2, we first summarize the AUC [Bradley, 1997] and ASR [Duan *et al.*, 2023] metrics for all baselines and PFAMI against two generative models over two datasets. In addition, we illustrate receiver operating characteristic (ROC) curves for PFAMI and the best baseline in Appendix A.3 for a more comprehensible presentation. From the aforementioned experimental results, the following analyses are summarized:

- PFAMI consistently outperforms all baseline methods in all scenarios:** The PFAMI_{NNs} and PFAMI_{Met} models achieve the highest average ASRs of 90.0% and 86.1% respectively. Furthermore, PFAMI exhibits approximate 35.9% improvement in AUC compared to the most competitive baseline on VAE, even when the baseline is set up with white-box access. Moreover, PFAMI_{NNs} achieves higher ASR and AUC compared to SecMI_{NNs} that assumes access to a large number of member and non-member data records of target models.
- The incremental performance provided by PFAMI_{NNs} verifies the necessity of exploring neighbor space with neural networks:** Compared with PFAMI_{Met}, PFAMI_{NNs} captures the variation of probabilistic fluctuations with neural networks can significantly increase the inference performance (about 5% and 3% improvement in ASR and AUC.).
- The overall low ASR and AUC of existing MIAs reveal their intractability on generative models without overfitting:** Most baselines, particularly those in the black-box setting, achieved low ASR, often comparable to random guesses. This phenomenon validates our claim that existing MIAs overly rely on overfitting in target models. Additionally, the high query frequency and computational overhead requirements further diminish the applicability and practicality of these MIAs.
- The diffusion model exposes more privacy risks due to its multi-step characteristic:** Compared to VAEs, both PFAMI_{NNs} and PFAMI_{Met} exhibit superior attack performance on diffusion model. This phenomenon can be attributed to the enhanced confidence in inferring mem-

Table 2: Performance of PFAMI across two generative models and two datasets. \uparrow represents that the higher the metric, the better of performance. **Bold** and Underline respectively denote the best and the second-best results for each metric. # Query indicates the number of query requests issued to the target model by each attack algorithm to complete an attack. N/A demonstrates that SecMI_{stat} and SecMI_{NNs} are unavailable on VAEs, since they are specially designed for diffusion models.

Attack Types	Method	# Query	DDPM				VAE			
			Celeba-64		Tiny-IN		Celeba-64		Tiny-IN	
			ASR \uparrow	AUC \uparrow	ASR \uparrow	AUC \uparrow	ASR \uparrow	AUC \uparrow	ASR \uparrow	AUC \uparrow
White-Box	Co-Membership Attack	1000	0.637	0.682	0.632	0.679	0.640	0.691	0.637	0.690
	GAN-Leaks (White-Box)	1000	0.623	0.601	0.618	0.593	0.601	0.586	0.595	0.582
Black-Box	Monte-Carlo Set	10000	0.500	0.502	0.500	0.501	0.501	0.502	0.501	0.501
	Over-Representation	10000	0.511	0.517	0.509	0.510	0.508	0.514	0.506	0.513
	LOGAN	10000	0.509	0.507	0.508	0.507	0.505	0.506	0.506	0.509
	GAN-Leaks (Black-Box)	10000	0.503	0.505	0.502	0.504	0.505	0.506	0.502	0.505
Gray-Box	SecMI _{stat}	12	0.690	0.741	0.673	0.729	N/A	N/A	N/A	N/A
	SecMI _{NNs}	12	0.791	0.867	0.783	0.859	N/A	N/A	N/A	N/A
	PFAMI _{Met}	20	<u>0.909</u>	<u>0.965</u>	<u>0.900</u>	<u>0.961</u>	<u>0.822</u>	<u>0.900</u>	<u>0.811</u>	<u>0.893</u>
	PFAMI _{NNs}	110	0.947	0.986	0.939	0.978	0.863	0.939	0.849	0.927

Table 3: PFAMI is compared with the best baseline in terms of performance against various generative models, where SecMI_{NNs} and Co-Membership Attack stand as the best baselines for diffusion models and VAEs. Models are trained over the Celeba-64 dataset.

Target Model	Best Baseline		PFAMI _{Met}		PFAMI _{NNs}	
	ASR \uparrow	AUC \uparrow	ASR \uparrow	AUC \uparrow	ASR \uparrow	AUC \uparrow
DDIM	0.799	0.871	0.913	0.969	0.952	0.987
PNDM	0.787	0.865	0.907	0.968	0.941	0.977
LDM	0.786	0.862	0.901	0.961	0.932	0.968
Beta-VAE	0.642	0.695	0.824	0.903	0.863	0.940
WAE	0.667	0.723	0.831	0.916	0.867	0.944
RHVAE	0.652	0.702	0.817	0.899	0.856	0.927

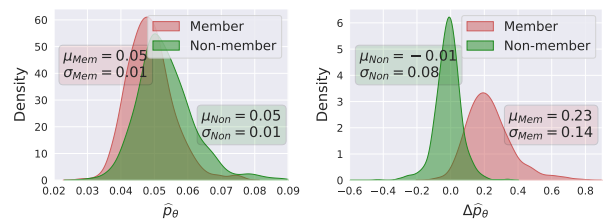
bership through the estimation of probability fluctuations across different time steps in diffusion models.

5.3 Generalizability Study

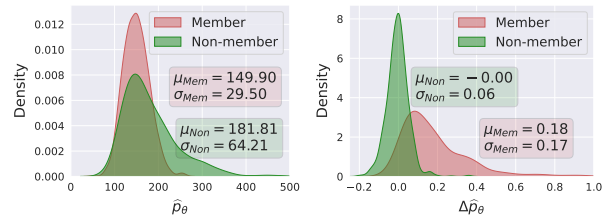
To validate the generalizability and robustness of our proposed attack method on probabilistic generative models, we consider six different generative models: DDIM [Song *et al.*, 2021], PNDM [Liu *et al.*, 2022] and LDM [Rombach *et al.*, 2022] as the variants of diffusion models. Beta-VAE [Higgins *et al.*, 2017], WAE [Tolstikhin *et al.*, 2018] and RHVAE [Chadebec *et al.*, 2023] as the variants of VAEs. As the results demonstrated in Table 3, our proposed method can achieve generally well attack performance across various generative models. Furthermore, the experimental results once again demonstrate the higher privacy exposure risk of diffusion models regarding MIAs. Additionally, we also evaluate our method and the most aggressive MIA designed for diffusion models on Stable Diffusion [Rombach *et al.*, 2022], one of the most prevalent and state-of-the-art conditional diffusion models. The details can be found in Appendix A.4.

5.4 How the Probabilistic Fluctuation Works

We conduct detailed investigations about how our proposed probabilistic fluctuation works as a qualified extractor to distinguish member and non-member records. As exhibited in Figure 3, we first visualize statistic distributions of the approximate probability \hat{p}_θ and our proposed probabilistic fluctuation $\Delta\hat{p}_\theta$ on member and non-member records. We found



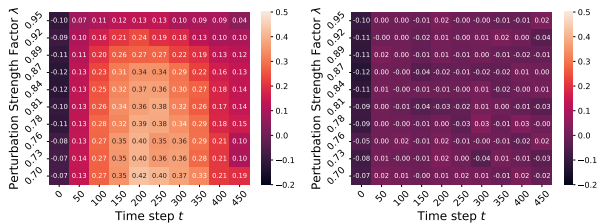
(a) Distributions of \hat{p}_θ (Left) and $\Delta\hat{p}_\theta$ (Right) in DDPM.



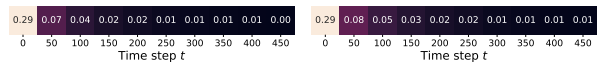
(b) Distributions of \hat{p}_θ (Left) and $\Delta\hat{p}_\theta$ (Right) in VAE.

Figure 3: The discrimination of member and non-member records over approximate probability \hat{p}_θ and approximate probabilistic fluctuation $\Delta\hat{p}_\theta$ on DDPM and VAE.

that just identifying the member records based on the approximate probability, as adopted by most existing works [Hilprecht *et al.*, 2019; Duan *et al.*, 2023], is not reliable. Especially when the target generative model is not overfitting, the probability for both member and non-member data is very close, especially in the diffusion model, where their distributions almost overlap entirely. On the contrary, when using the probability fluctuation we designed, the obtained results have more substantial discriminative power. Specifically, due to the memorization effect, members are peak points in the probability distribution, and their neighbors tend to have lower probabilities. Hence, our designed probability fluctuation metric would be greater than zero. Conversely, non-members are typically located near inflection points in the generation probability distribution, resulting in a stable probability fluctuation around zero. These experimental results also demonstrate that PFAMI_{Met} can effectively enhance the discrimina-



(a) $\Delta \hat{p}_\theta$ on member (Left) and non-member (Right).



(b) \hat{p}_θ on member (Left) and non-member (Right).

Figure 4: The visualization of the probabilistic fluctuation $\Delta \hat{p}_\theta$ and the approximate probability \hat{p}_θ for member and non-member records on DDPM trained with Celeba-64.

Table 4: Results of ablation study on the Celeba-64 dataset.

Methods	DDPM		VAE	
	ASR \uparrow	AUC \uparrow	ASR \uparrow	AUC \uparrow
PFAMI _{NNs}	0.947	0.986	0.863	0.939
w/o Variational Probability Assessment	0.537	0.541	0.523	0.532
w/o Neighbor Records Sampling	0.694	0.781	0.677	0.747
w/o NNs-based Inference Function	0.909	0.965	0.822	0.900

tion between member and non-member records, making it easier to establish a threshold as a criterion for measuring record membership.

We also visualize the figure of probabilistic fluctuation $\Delta \hat{p}_\theta$ on diffusion models to help understand why the NNs-based approach can further improve the attack performance. As shown in Figure 4(a), we can observe an overall positive probability fluctuation of member records, except there are also apparent regular variations of probabilistic fluctuation over time step and perturbation strength. Consequently, this variation further benefits the NNs-based approach to extract the difference between member and non-member records. In contrast, as shown in Figure 4(b), the member and non-member records are indistinguishable only with the approximate probability on sampled time steps.

5.5 Ablation Study

We conduct an ablation study to investigate the performance gain provided by each module. Specifically, we respectively remove the variational probability assessment and neighbor record sampling modules as we introduced in Sec. 4.2 and Sec. 4.3. Then we remove the NNs-based inference function proposed in Sec. 4.4. The results are presented in Table 4, where each module demonstrates significant improvement in performance gain, and the combination of all modules achieves the highest ASR of PFAMI_{NNs}. The results also suggested that the approximate probability assessment is the basis of probabilistic fluctuation. Without this, it is difficult for our method to accurately estimate the fluctuation of generative probabilities, resulting in poor attack effectiveness.

6 Conclusion

In this article, we first point out that existing MIA algorithms largely rely on overfitting in generative models, which can be avoided by several regularization methods. Thus, the performance of these MIAs cannot be guaranteed. To mitigate this flaw, we opt for a more general phenomenon: memorization. Memorization is inevitable in deep learning models, and we have found that this phenomenon can be detected in probabilistic generative models by estimating the probabilistic fluctuations within the local scope of the target records. Therefore, we present a Probabilistic Fluctuation Assessing Membership Inference Attack (PFAMI) based on the distinct probabilistic fluctuation characteristics of members and non-members. We conduct comprehensive experiments to evaluate PFAMI with various baselines on diffusion models and VAEs across different datasets. The results demonstrate that PFAMI maintains higher ASR and robustness across various scenarios than all baselines. We leave extending our attack framework to GAN as the future works, where we may incorporate the samples from the generator and the confidence values from the discriminator to design a better method.

References

- [Bommasani *et al.*, 2021] Rishi Bommasani, Drew A. Hudson, Ehsan Adeli, Russ B. Altman, Simran Arora, Sydney von Arx, Michael S. Bernstein, and et al. On the opportunities and risks of foundation models. *ArXiv preprint*, abs/2108.07258, 2021.
- [Bradley, 1997] Andrew P Bradley. The use of the area under the roc curve in the evaluation of machine learning algorithms. *Pattern recognition*, 30(7):1145–1159, 1997.
- [Carlini *et al.*, 2023] Nicolas Carlini, Jamie Hayes, Milad Nasr, Matthew Jagielski, Vikash Sehwal, Florian Tramèr, Borja Balle, Daphne Ippolito, and Eric Wallace. Extracting Training Data from Diffusion Models. In *32nd USENIX Security Symposium (USENIX Security 23)*, pages 5253–5270, 2023.
- [Chadebec *et al.*, 2023] Clément Chadebec, Elina Thibeau-Sutre, Ninon Burgos, and Stéphanie Allasonnière. Data Augmentation in High Dimensional Low Sample Size Setting Using a Geometry-Based Variational Autoencoder. *IEEE Transactions on Pattern Analysis and Machine Intelligence*, 45(3):2879–2896, 2023.
- [Chen *et al.*, 2020] Dingfan Chen, Ning Yu, Yang Zhang, and Mario Fritz. GAN-Leaks: A Taxonomy of Membership Inference Attacks against Generative Models. In *Proceedings of the 2020 ACM SIGSAC Conference on Computer and Communications Security, CCS ’20*, pages 343–362, New York, NY, USA, 2020. Association for Computing Machinery.
- [Choquette-Choo *et al.*, 2021] Christopher A. Choquette-Choo, Florian Tramèr, Nicolas Carlini, and Nicolas Papernot. Label-only membership inference attacks. In *Proceedings of the 38th International Conference on Machine Learning, ICML 2021, 18-24 July 2021, Virtual Event*, volume 139 of *Proceedings of Machine Learning Research*, pages 1964–1974. PMLR, 2021.

- [Duan *et al.*, 2023] Jinhao Duan, Fei Kong, Shiqi Wang, Xiaoshuang Shi, and Kaidi Xu. Are Diffusion Models Vulnerable to Membership Inference Attacks? In *Proceedings of the 38th International Conference on Machine Learning, ICML 2023*. PMLR, February 2023.
- [Dwivedi *et al.*, 2023] Yogesh K. Dwivedi, Nir Kshetri, and Laurie *et al.* Hughes. Opinion Paper: “So what if ChatGPT wrote it?” Multidisciplinary perspectives on opportunities, challenges and implications of generative conversational AI for research, practice and policy. *International Journal of Information Management*, 71:102642, 2023.
- [Epstein *et al.*, 2023] Ziv Epstein, Aaron Hertzmann, Investigators of Human Creativity, Memo Akten, Hany Farid, Jessica Fjeld, Morgan R Frank, Matthew Groh, Laura Herman, Neil Leach, *et al.* Art and the science of generative ai. *Science*, 380(6650):1110–1111, 2023.
- [Feldman and Zhang, 2020] Vitaly Feldman and Chiyuan Zhang. What neural networks memorize and why: Discovering the long tail via influence estimation. In Hugo Larochelle, Marc’Aurelio Ranzato, Raia Hadsell, Maria-Florina Balcan, and Hsuan-Tien Lin, editors, *Advances in Neural Information Processing Systems 33: Annual Conference on Neural Information Processing Systems 2020, NeurIPS 2020, December 6-12, 2020, virtual*, 2020.
- [Feldman, 2020] Vitaly Feldman. Does learning require memorization? a short tale about a long tail. In *Proceedings of the 52nd Annual ACM SIGACT Symposium on Theory of Computing, STOC 2020, Chicago, IL, USA, June 22-26, 2020*, pages 954–959. ACM, 2020.
- [Hayes *et al.*, 2019] Jamie Hayes, Luca Melis, George Danezis, and Emiliano De Cristofaro. LOGAN: Membership Inference Attacks Against Generative Models. *Proceedings on Privacy Enhancing Technologies*, 2019(1):133–152, 2019.
- [He *et al.*, 2016] Kaiming He, Xiangyu Zhang, Shaoqing Ren, and Jian Sun. Deep residual learning for image recognition. In *2016 IEEE Conference on Computer Vision and Pattern Recognition, CVPR 2016, Las Vegas, NV, USA, June 27-30, 2016*, pages 770–778. IEEE Computer Society, 2016.
- [Higgins *et al.*, 2017] Irina Higgins, Loïc Matthey, Arka Pal, Christopher Burgess, Xavier Glorot, Matthew Botvinick, Shakir Mohamed, and Alexander Lerchner. beta-vae: Learning basic visual concepts with a constrained variational framework. In *5th International Conference on Learning Representations, ICLR 2017, Toulon, France, April 24-26, 2017, Conference Track Proceedings*. OpenReview.net, 2017.
- [Hilprecht *et al.*, 2019] Benjamin Hilprecht, Martin Härterich, and Daniel Bernau. Monte Carlo and Reconstruction Membership Inference Attacks against Generative Models. *Proc. Priv. Enhancing Technol.*, 2019(4):232–249, 2019.
- [Ho *et al.*, 2020] Jonathan Ho, Ajay Jain, and Pieter Abbeel. Denoising diffusion probabilistic models. In Hugo Larochelle, Marc’Aurelio Ranzato, Raia Hadsell, Maria-Florina Balcan, and Hsuan-Tien Lin, editors, *Advances in Neural Information Processing Systems 33: Annual Conference on Neural Information Processing Systems 2020, NeurIPS 2020, December 6-12, 2020, virtual*, 2020.
- [Hu and Pang, 2021] Hailong Hu and Jun Pang. Membership Inference Attacks against GANs by Leveraging Overrepresentation Regions. In *Proceedings of the 2021 ACM SIGSAC Conference on Computer and Communications Security, CCS ’21*, pages 2387–2389, New York, NY, USA, 2021. Association for Computing Machinery.
- [Hu *et al.*, 2022] Hongsheng Hu, Zoran Salcic, Lichao Sun, Gillian Dobbie, Philip S. Yu, and Xuyun Zhang. Membership Inference Attacks on Machine Learning: A Survey. *ACM Computing Surveys*, 54(11s):235:1–235:37, 2022.
- [Kingma and Ba, 2015] Diederik P. Kingma and Jimmy Ba. Adam: A method for stochastic optimization. In Yoshua Bengio and Yann LeCun, editors, *3rd International Conference on Learning Representations, ICLR 2015, San Diego, CA, USA, May 7-9, 2015, Conference Track Proceedings*, 2015.
- [Kingma and Welling, 2014] Diederik P. Kingma and Max Welling. Auto-encoding variational bayes. In Yoshua Bengio and Yann LeCun, editors, *2nd International Conference on Learning Representations, ICLR 2014, Banff, AB, Canada, April 14-16, 2014, Conference Track Proceedings*, 2014.
- [Le and Yang, 2015] Ya Le and Xuan Yang. Tiny imagenet visual recognition challenge. *CS 231N*, 7(7):3, 2015.
- [Li *et al.*, 2021] Junyi Li, Tianyi Tang, Wayne Xin Zhao, and Ji-Rong Wen. Pretrained Language Model for Text Generation: A Survey. In *Proceedings of the Thirtieth International Joint Conference on Artificial Intelligence*, pages 4492–4499, Montreal, Canada, 2021. International Joint Conferences on Artificial Intelligence Organization.
- [Liu *et al.*, 2015] Ziwei Liu, Ping Luo, Xiaogang Wang, and Xiaoou Tang. Deep learning face attributes in the wild. In *2015 IEEE International Conference on Computer Vision, ICCV 2015, Santiago, Chile, December 7-13, 2015*, pages 3730–3738. IEEE Computer Society, 2015.
- [Liu *et al.*, 2019] Kin Sum Liu, Chaowei Xiao, Bo Li, and Jie Gao. Performing Co-membership Attacks Against Deep Generative Models. In *2019 IEEE International Conference on Data Mining (ICDM)*, pages 459–467, 2019.
- [Liu *et al.*, 2022] Luping Liu, Yi Ren, Zhijie Lin, and Zhou Zhao. Pseudo numerical methods for diffusion models on manifolds. In *The Tenth International Conference on Learning Representations, ICLR 2022, Virtual Event, April 25-29, 2022*. OpenReview.net, 2022.
- [Loshchilov and Hutter, 2019] Ilya Loshchilov and Frank Hutter. Decoupled weight decay regularization. In *7th International Conference on Learning Representations, ICLR 2019, New Orleans, LA, USA, May 6-9, 2019*. OpenReview.net, 2019.

- [Mattern *et al.*, 2023] Justus Mattern, Fatemehsadat Mireshghallah, Zhijing Jin, Bernhard Schölkopf, Mrinmaya Sachan, and Taylor Berg-Kirkpatrick. Membership Inference Attacks against Language Models via Neighbourhood Comparison, 2023.
- [Oussidi and Elhassouny, 2018] Achraf Oussidi and Azedine Elhassouny. Deep generative models: Survey. In *2018 International Conference on Intelligent Systems and Computer Vision (ISCV)*, pages 1–8, 2018.
- [Pang and Wang, 2023] Yan Pang and Tianhao Wang. Black-box membership inference attacks against fine-tuned diffusion models. *arXiv preprint arXiv:2312.08207*, 2023.
- [Rombach *et al.*, 2022] Robin Rombach, Andreas Blattmann, Dominik Lorenz, Patrick Esser, and Björn Ommer. High-Resolution Image Synthesis With Latent Diffusion Models. In *Proceedings of the IEEE/CVF Conference on Computer Vision and Pattern Recognition*, pages 10684–10695, 2022.
- [Ronneberger *et al.*, 2015] Olaf Ronneberger, Philipp Fischer, and Thomas Brox. U-net: Convolutional networks for biomedical image segmentation. In *Medical Image Computing and Computer-Assisted Intervention—MICCAI 2015: 18th International Conference, Munich, Germany, October 5-9, 2015, Proceedings, Part III 18*, pages 234–241. Springer, 2015.
- [Shokri *et al.*, 2017] Reza Shokri, Marco Stronati, Congzheng Song, and Vitaly Shmatikov. Membership Inference Attacks Against Machine Learning Models. In *2017 IEEE Symposium on Security and Privacy (SP)*, pages 3–18, 2017.
- [Song *et al.*, 2021] Jiaming Song, Chenlin Meng, and Stefano Ermon. Denoising diffusion implicit models. In *9th International Conference on Learning Representations, ICLR 2021, Virtual Event, Austria, May 3-7, 2021*. OpenReview.net, 2021.
- [Stokel-Walker and Van Noorden, 2023] Chris Stokel-Walker and Richard Van Noorden. What ChatGPT and generative AI mean for science. *Nature*, 614(7947):214–216, 2023.
- [Tashiro *et al.*, 2021] Yusuke Tashiro, Jiaming Song, Yang Song, and Stefano Ermon. CSDI: conditional score-based diffusion models for probabilistic time series imputation. In Marc’Aurelio Ranzato, Alina Beygelzimer, Yann N. Dauphin, Percy Liang, and Jennifer Wortman Vaughan, editors, *Advances in Neural Information Processing Systems 34: Annual Conference on Neural Information Processing Systems 2021, NeurIPS 2021, December 6-14, 2021, virtual*, pages 24804–24816, 2021.
- [Tolstikhin *et al.*, 2018] Ilya O. Tolstikhin, Olivier Bousquet, Sylvain Gelly, and Bernhard Schölkopf. Wasserstein auto-encoders. In *6th International Conference on Learning Representations, ICLR 2018, Vancouver, BC, Canada, April 30 - May 3, 2018, Conference Track Proceedings*. OpenReview.net, 2018.
- [van Breugel *et al.*, 2023] Boris van Breugel, Hao Sun, Zhaozhi Qian, and Mihaela van der Schaar. Membership Inference Attacks against Synthetic Data through Overfitting Detection. In *Proceedings of The 26th International Conference on Artificial Intelligence and Statistics*, pages 3493–3514. PMLR, April 2023.
- [van den Burg and Williams, 2021] Gerrit J. J. van den Burg and Chris Williams. On memorization in probabilistic deep generative models. In Marc’Aurelio Ranzato, Alina Beygelzimer, Yann N. Dauphin, Percy Liang, and Jennifer Wortman Vaughan, editors, *Advances in Neural Information Processing Systems 34: Annual Conference on Neural Information Processing Systems 2021, NeurIPS 2021, December 6-14, 2021, virtual*, pages 27916–27928, 2021.
- [Ying, 2019] Xue Ying. An overview of overfitting and its solutions. In *Journal of physics: Conference series*, volume 1168, page 022022. IOP Publishing, 2019.
- [Zhai *et al.*, 2018] Junhai Zhai, Sufang Zhang, Junfen Chen, and Qiang He. Autoencoder and its various variants. In *2018 IEEE international conference on systems, man, and cybernetics (SMC)*, pages 415–419. IEEE, 2018.
- [Zhang *et al.*, 2020] Yuheng Zhang, Ruoxi Jia, Hengzhi Pei, Wenxiao Wang, Bo Li, and Dawn Song. The Secret Revealer: Generative Model-Inversion Attacks Against Deep Neural Networks. In *Proceedings of the IEEE/CVF Conference on Computer Vision and Pattern Recognition*, pages 253–261, 2020.

Ethical Statement and Broader Impacts

In this paper, we propose a membership inference attack method, PFAMI, which can be maliciously utilized to infer the privacy of a specific individual whose data has been collected to train a probabilistic generative model. Indeed, we acknowledge that PFAMI can bring considerable privacy risk to existing generative models. Thus, to mitigate the potential abuse of this research, all experimental results are concluded over widely adopted public datasets, guaranteeing that each member record we extract has already been exposed to the public, thus avoiding any additional privacy breaches. In addition, we have made our code publicly available to facilitate further research in finding suitable defense solutions. Therefore, we believe our paper can encourage future studies to consider not only the generative capabilities of models but also the aspect of public data privacy and security.

A Appendix

A.1 Key Notations of This Work

Table 5: Notations and descriptions.

Notation	Description
$\mathbf{x}^{(i)}$	A specific data record.
$\tilde{\mathbf{x}}_j^{(i)}$	A neighbor record of the target record $\mathbf{x}^{(i)}$.
$m^{(i)}$	The membership of the data record $\mathbf{x}^{(i)}$, 1 represents member, whereas 0 represents non-member.
θ	The parameters of the target generative model.
$\mathcal{A}(\mathbf{x}^{(i)}, \theta)$	The adversary algorithm for MIA.
$p_\theta(\mathbf{x}^{(i)})$	The probability of record $\mathbf{x}^{(i)}$ being generated by the generative model θ .
$\hat{p}_\theta(\mathbf{x}^{(i)})$	The approximate value of probability $p_\theta(\mathbf{x}^{(i)})$.
$\Delta\hat{p}_\theta(\mathbf{x}^{(i)}, \tilde{\mathbf{x}}_j^{(i)})$	The probabilistic fluctuation between the target record $\mathbf{x}^{(i)}$ and one of its neighbor $\tilde{\mathbf{x}}_j^{(i)}$.
$\mathcal{M}(\cdot, \lambda_j)$	The perturbation mechanism.
$\{\lambda_j\}_{j=1}^M$	The sequence of perturbation strengths.
N	The query times for estimating $\hat{p}_\theta(\mathbf{x}^{(i)})$.
M	The sampled number of neighbor records.
$\Delta\hat{p}_\theta(\mathbf{x}^{(i)})$	The $M \times N$ probabilistic fluctuation figure of the target record $\mathbf{x}^{(i)}$.

A.2 Detailed Information for Reproduction

Implementation Details

All target models are trained with general settings, and the backbone of diffusion models and VAEs are selected to UNet [Ronneberger *et al.*, 2015] and ResNet [He *et al.*, 2016]. The step length of diffusion models is set to $T = 1,000$, and the dimension of latent variables \mathbf{z} in VAEs is set to 64. To assure the target models are well-generalized, we use AdamW [Loshchilov and Hutter, 2019] to optimize all generative models, which fuses the Adam optimizer [Kingma and Ba, 2015] and the L2 regularization to reduce the risk of model overfitting. Furthermore, we adopt early-stopping during the training process, where we stop training before the loss increases in the validation set. The crop is adopted as the default perturbation mechanism for all experiments. For PFAMI_{Met}, we set $N = 10$ and $M = 1$ for attacking against both diffusion models and VAEs. In diffusion models, we sample time steps starting from 0 to 500 with an interval of 50, as we found that the probabilistic fluctuations of member and non-member are indistinguishable in the later time steps. As the larger the time step, the closer the image is to Gaussian noise. As for PFAMI_{NNs}, we designed a set of equally spaced increasing perturbation strengths, the factor λ ranging from 0.98 to 0.7, with a length of $M = 10$. We choose the ResNet [He *et al.*, 2016] as the backbone of attack model $f_{\mathcal{A}}$ and train it with only 2,000 samples provided by the shadow model.

Datasets

The detailed split and other information of the two datasets, Celeba-64 and Tiny-IN, are summarized in Table 6.

Target Models

The target models are all prepared with the two most popular generative model libraries: diffusers and pythae, which allows researchers to easily deploy our attack model on other generative models with just a few lines of code modification. All diffusion models, including DDPM, DDIM, PNDM, and LDM are deployed with diffusers, and trained in 500 epochs with a learning rate of 0.0001 and batch size of 16. All VAEs, including the vanilla VAE, Beta-VAE, WAE, and RHVAE, are deployed with pythae, and trained in 100 epochs with a learning rate of 0.0001 and batch size of 100. Note that the training process will be interrupted early if the loss starts to increase in the evaluation set.

A.3 The ROC Curves of PFAMI and Aggressive Baselines

As a supplement to the main experimental results shown in Table 2, we also provide the raw ROC curve for a more straightforward presentation in Figure 5.

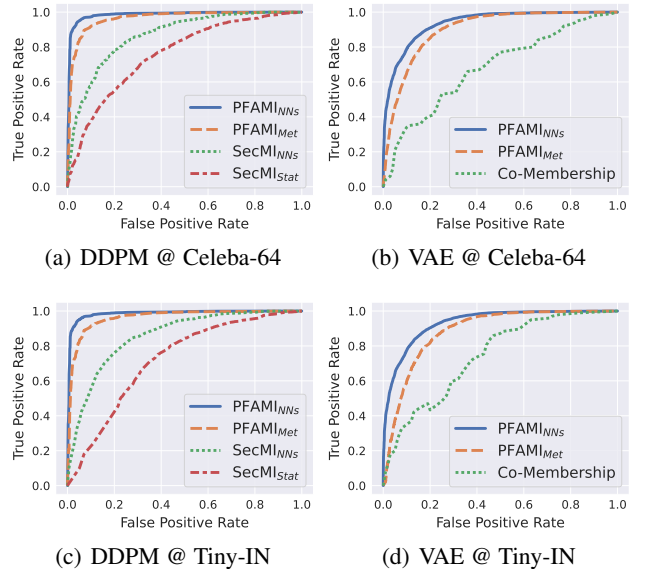


Figure 5: ROC curves of PFAMI and the best baselines on two generative models trained in Celeba-64 and Tiny-IN datasets.

A.4 Performance Appraisal on Stable Diffusion

We assess the performance of PFAMI and the most aggressive baseline, SecMI [Duan *et al.*, 2023], on the extremely state-of-the-art conditional diffusion model [Rombach *et al.*, 2022], Stable Diffusion, over the Pokemon dataset. In contrast to unconditional diffusion models and VAEs that are trained from scratch, we follow the same setup as Duan *et al.* to fine-tune the Stable Diffusion based on the pre-trained

Table 6: Detailed split and other information of datasets.

Dataset	Resolution	Target Model		Shadow Model		Reference Model	
		# Member	# Non-member	# Member	# Non-member	# Member	# Non-member
Celeba-64	64	50,000	10,000	50,000	10,000	50,000	10,000
Tiny-IN	64	30,000	5,000	30,000	5,000	30,000	5,000

model released in the HuggingFace². The results are summarized in Table 7, where PFAMI still strikes notable inference performances.

Table 7: Inference Performance of PFAMI_{Met} and the most aggressive baselines, SecMI_{Stat}, on Stable Diffusion.

Method	ASR \uparrow	AUC \uparrow	TPR@1%FPR \uparrow
PFAMI _{Met}	0.967	0.993	0.774
SecMI _{Stat}	0.817	0.886	0.145

A.5 Hyperparameters Learning

Perturbation Mechanism

In this paper, the perturbation mechanism is a key module in PFAMI for characterizing the overall probabilistic fluctuation around the target record, which helps the attacker to sample representative neighbor records of the target record. Therefore, we investigate what perturbation mechanisms will be appropriate for PFAMI to achieve better performances. Inspired by existing data augmentation techniques, we have studied two different types of data augmentation techniques, namely, color-based and geometry-based. They respectively involve various operations such as brightness, contrast, saturation, hue, as well as cropping, rotation, perspective, padding. We present several metrics to evaluate each perturbation mechanism. Except for ASR and AUC, we also consider TPR @ 1% FPR, i.e., the TPR when FPR is 1%. It can more accurately evaluate the attack performance when most mechanisms achieve a near-perfect AUC of approximately 0.9 and ASR scores. The results are shown in Table 8, from which we can observe that the crop combines excellent performance and stability. Therefore, we adopt crop as the default perturbation mechanism in all experiments. The results are presented in Table 8, which illustrates that the crop demonstrates remarkable performance and robustness over two generative models. Consequently, the crop is selected as the default perturbation mechanism for all experimental trials.

Table 8: Performance of PFAMI_{Met} on DDPM@Celeba-64 with different perturbation techniques.

Perturbation Techniques		DDPM			VAE		
		ASR	AUC	TPR @ 1% FPR	ASR	AUC	TPR @ 1% FPR
Color	Brightness	0.855	0.920	0.291	0.843	0.919	0.237
	Contrast	0.858	0.918	0.192	0.835	0.909	0.165
	Saturation	0.681	0.741	0.044	0.683	0.753	0.033
	Hue	0.851	0.927	0.379	0.777	0.855	0.104
Geometry	Crop	0.909	0.965	0.468	0.834	0.912	0.229
	Rotation	0.917	0.968	0.574	0.806	0.879	0.119
	Perspective	0.836	0.911	0.167	0.730	0.799	0.049
	Downsampling	0.838	0.910	0.297	0.830	0.909	0.156

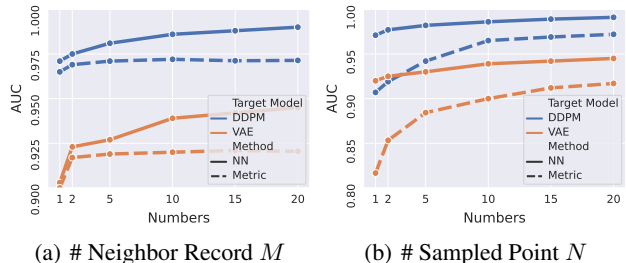


Figure 6: The attack performances against DDPM and VAE on Celeba-64 w.r.t the number of queries.

Impact of the Query Times

We investigate the impact of query numbers on the performance of PFAMI attacks from two perspectives: the number of neighbor records M and the number of sampled points N . Furthermore, we have conducted a detailed investigation into the variations in attack performance with respect to query numbers, considering different attack strategies and different architectures of generative models. Note that the default number of neighbor records M is repetitively set to 1 and 10 in PFAMI_{Met} and PFAMI_{NNs}, and the default number of sampled points N is set to 10. As the results presented in Figure 6, the attack performance of the NN-based strategy is exceptionally stable, due to the integration of probabilistic fluctuations from multiple directions. On the other hand, the attack strategy based on statistical metric tends to rely more on the number of samples and generally achieve a good balance between performance and efficiency with around 10 sampled numbers.

A.6 Interpretation of Probabilistic Fluctuation as Directional Second Derivative

In multivariable calculus, the second partial derivative test is generally utilized to authenticate whether a critical point is a local maxima, minima, or saddle point. From the inherent concept of this work, the member record is believed to be located on the local maximum of the probability distribution, where the Hessian matrix is negative definite, i.e., all the directional second derivatives are negative. However, it is intractable to determine whether all second-order directional derivatives of a sample x are negative. Moreover, we need only an approximate judgment in the region of local maxima, rather than strictly defined mathematical critical points. Therefore, we consider estimating the position of record x in the probability distribution by its expected value of second-

²<https://huggingface.co/CompVis/stable-diffusion-v1-4>

order directional derivatives:

$$\mathbb{E}_{\mathbf{z}} (\partial_{uu}^2 p_{\theta}(\mathbf{x})) = \mathbb{E}_{\mathbf{z}} (\mathbf{z}^{\top} H_p(\mathbf{x}) \mathbf{z}), \quad (21)$$

where $H_p(\cdot)$ represents the hessian matrix of the probability function $p_{\theta}(\cdot)$ parameterized by the generative model θ . This expression can be further approximated with the symmetric form:

$$\mathbf{z}^{\top} H_p(\mathbf{x}) \mathbf{z} \approx \frac{p_{\theta}(\mathbf{x} + h\mathbf{z}) + p_{\theta}(\mathbf{x} - h\mathbf{z}) - 2p_{\theta}(\mathbf{x})}{h^2}, \quad (22)$$

where requires $h \rightarrow 0$, and \mathbf{z} can be considered as "perturbation shift". Thus, $\mathbf{x} \pm h\mathbf{z}$ can be regarded as neighbor text records of \mathbf{x} in the data distribution. From a statistical perspective, it is reasonable to assume that this "shift" is symmetric around the center of \mathbf{x} , then we further omit the factor h and simplify Eq. 21 as follows:

$$\begin{aligned} \mathbb{E}_{\mathbf{z}} (\partial_{uu}^2 p_{\theta}(\mathbf{x})) &= \mathbb{E}_{\mathbf{z}} (p_{\theta}(\mathbf{x} + \mathbf{z}) - p_{\theta}(\mathbf{x})) \\ &= \mathbb{E}_{\tilde{\mathbf{x}} \sim q(\cdot | \mathbf{x})} (p_{\theta}(\tilde{\mathbf{x}}) - p_{\theta}(\mathbf{x})), \end{aligned} \quad (23)$$

where $q(\cdot | \mathbf{x})$ is a perturbation function that gives a distribution over $\tilde{\mathbf{x}}$, mildly shift the original image \mathbf{x} and maintain the outline and key features, which aligns with Eq. (22) that requires the perturbation $h \rightarrow 0$. Then, we can approximate Eq. 23 through Monte Carlo sampling:

$$\begin{aligned} \mathbb{E}_{\mathbf{z}} (\partial_{uu}^2 p_{\theta}(\mathbf{x})) &= \frac{1}{M} \sum_{j=1}^M p_{\theta}(\tilde{\mathbf{x}}_j) - p_{\theta}(\mathbf{x}) \\ &\propto -\frac{1}{M} \sum_{j=1}^M \Delta p_{\theta}(\mathbf{x}, \tilde{\mathbf{x}}_j), \end{aligned} \quad (24)$$

which is exactly the overall probabilistic fluctuation measured in Eq. (19).